https://doi.org/10.5194/egusphere-2024-3220
Preprint. Discussion started: 4 February 2025

Implementation of an intermediate complexity snow-physics scheme (ISBA-Explicit Snow) into a sea-ice model (SI³): 1D thermodynamic coupling and validation.

Théo Brivoal[1], Virginie Guemas[1], Martin Vancoppenole[2], Clément Rousset[2], Bertrand Decharme[1]

[1] Centre National de Recherches Météorologiques (CNRM), Météo-France, CNRS, Université de Toulouse, Toulouse, France
[2] LOCEAN-IPSL, CNRS, Sorbonne Université, Paris, France

Correspondence to: Théo Brivoal (theo.brivoal@meteo.fr)

Abstract.

Snow plays a crucial role in the formation and sustainability of sea ice. Due to its thermal properties, snow acts as an insulating layer, shielding the ice from the air above. This insulation reduces the heat transfer between the sea-ice and the atmosphere. Due to its reflective properties, the snow cover also strongly contributes to albedo over ice-covered regions, which gives it a significant role in the earth's climate system.

Current state-of-art climate models use over-simple representations of the snow cover overlaying the sea ice. The snow cover is often represented with a one-layer scheme, assuming a constant density, no wet or dry metamorphism or assuming that no liquid water is stored in the snow. Here we implemented an intermediate complexity snow-physics scheme (ISBA-Explicit Snow) into a sea-ice model (SI³), which serves as the sea-ice component for upcoming versions of the CNRM-CM climate model. This is, to our knowledge, the first time that a snow model with such level of complexity is incorporated into a sea-ice model designed for global to regional applications. We validated our model comparing 1D simulations with data from the Surface Heat Budget of the Arctic Ocean (SHEBA) but also simulations from another advanced snow-on-sea-ice model (SnowModel-LG), and simulations with the previous SI³ snow scheme.

Our model simulates realistic snow thicknesses, densities, and temperatures, aligning well with SHEBA observations and SnowModel-LG outputs, while capturing their temporal variability. We show that the thickness, density, and conductivity of the snowpack are significantly affected by the choices made in parameterization for calculating snowfall density, wind-induced snow compaction, and by the choice of the atmospheric forcing. Unlike the previous SI³ snow scheme that assumed constant density and thermal conductivity, our model realistically simulates the evolution of these properties, resulting in more accurate temperatures at the snow-ice interface. Ultimately, our study shows that modelling the temporal changes in the density and thermal conductivity of the snow layers leads to a more accurate representation of heat transfer between the underlying sea ice and the atmosphere.

https://doi.org/10.5194/egusphere-2024-3220
Preprint. Discussion started: 4 February 2025

1 Introduction

Snow is an important component of the climate system. Due to its reflective properties, it regulates the earth's energy balance. Without snow, our planet would warm due to a positive feedback loop on the ocean, land, and atmosphere system (Webster et al., 2018). In the polar regions, snow accumulated on top of the sea-ice, leading to an increase of the surface albedo by up to 50% with respect to the bare ice albedo (e.g: Perovich and Polashenski, 2012) and to a reduction of the solar radiation absorbed by the sea-ice (and thus the climate system). Conversely, snow on sea ice acts as an insulator (e.g: Sturm and Massom, 2017), reducing the heat transfer between the sea-ice and the atmosphere and delaying the ice thermodynamic thickening, keeping the ice warm and thus thin (Fichefet et al., 2000; Lecomte et al., 2013). Snow can also promote sea ice growth, through the formation of superimposed ice (the refreezing of fresh percolating meltwater on top of sea ice, Nicolaus et al., 2003) and snow ice (refrozen mixture of snow and salt water flooding the base of the snow, Jutras et al., 2016). Despite its importance, snow on sea-ice remains an understudied component of the climate system.

The optical and thermal properties of snow are influenced by a multitude of processes that vary significantly in their frequency, magnitude, and occurrence across seasons, regions, and hemispheres (see Webster et al., 2018 and Sturm and Massom, 2017 for recent reviews). At microscopic scale, the freshly deposited snow undergoes complex metamorphic processes that modifies its grain size and density, thus impacting its thermal conductivity (Sturm et al., 1997) and albedo (Bohren and Beschta, 1979). After snowfall, the wind erodes or drifts the unconsolidated snow, shaping the heterogeneity of the snow cover in accordance with the sea-ice topography. A part of this blowing snow may also fall into leads, open cracks or polynyas where it may melt, form slush or refreeze (Leonard and Maksym, 2011). Wind also tends to compact the snowpack, thus increasing its density (Sommer et al., 2018).

Accurately representing snow on sea ice in climate models is crucial for capturing the complex interactions and feedbacks within the climate system, and for ensuring more reliable predictions of future climate changes (Fichefet et al., 2000; Holland et al., 2021; Lecomte et al., 2013). For instance, Fichefet et al. (2000) showed that reducing by half the thermal conductivity of the snow overlaying the Antarctic sea ice in a global coarse-resolution ice-ocean model significantly decreases the sea-ice thickness. They also observed changes in the stratification of the Southern Ocean and a weakening of the Antarctic Bottom Water meridional overturning. Similarly, in the Arctic, Lecomte et al. (2013) showed that using a constant snow conductivity in a coupled sea-ice / ocean model leads to an overestimation of sea-ice thickness in the Arctic. More recently, Holland et al. (2021) showed that increasing snow precipitation in climate models results in significant changes to sea-ice thickness, emphasizing the critical need for an accurate representation of the snow cover on sea ice within coupled Earth system models. While current state-of-the-art climate models employ relatively complex snow schemes over land, the scarcity of observations and the technical challenges involved in coupling snow with sea ice (Liston et al., 2020) lead to relying on over-simplistic representations of the snow on sea-ice in contrast to the more complex snow schemes employed over land. Indeed, snow on sea-ice in climate models is typically depicted using a simplified 1-layer scheme, assuming constant snow density and thermal conductivity, with no consideration for liquid water retention or snow metamorphism.

https://doi.org/10.5194/egusphere-2024-3220
Preprint. Discussion started: 4 February 2025

Over the recent years, efforts have been made towards using more complex snow models over the sea-ice. These models are mainly designed to produce datasets of snow properties such as (primarily) its thickness or (secondarily) density, to compensate for the lack of observational data and/or assist with remote sensing (the snow thickness is a required input to derive the sea-ice thickness from satellite altimetry). For example, Liston et al. (2020) developed for such applications a lagrangian snow model (SnowModel-LG) which follows the ice motion and includes a representation of snow density and grain size evolution, blowing-snow sublimation, snow melt and superimposed ice formation. Similarly, Wever et al. (2020) developed a sea-ice module for the unidimensional, physics-based, detailed, multi-layer snow cover model SNOWPACK, which they used in a Lagrangian framework.

Such lagrangian models are useful to improve the knowledge of the interactions between snow and sea-ice but are hardly suitable for climate systems that use an eulerian framework. Simple modelling of snow on sea ice with an eulerian framework has also been achieved. Lecomte et al. (2013) developed a parameterization that consists of a set of two linear equations relating the snow thermal conductivity and density to the mean seasonal wind speed. More recently, Petty et al. (2018) developed an eulerian model which uses two snow layers, a rather simple parametrization representing accumulation, wind packing, advection–divergence, blowing snow lost to leads to represent key sources and sinks of snow on sea ice.

The sea-ice component for upcoming versions of the CNRM climate model (CNRM-CM, Voldoire et al., 2013), called SI³ (Sea Ice modeling Integrated Initiative, Vancoppenolle et al., 2023) incorporates a simplistic representation of snow over sea ice, assuming a constant density and thermal conductivity and a constant. In this study, we integrate a more advanced snow scheme, ISBA-Explicit Snow, (ISBA-ES, Boone and Etchevers, 2001) into SI³ to improve its representation of the snow over sea-ice. The ISBA-ES snow model incorporates detailed representations of snowpack properties such as density, grain size, and thermal conductivity, allowing for more accurate (than previous SI³ versions) simulation of snow accumulation, compaction, metamorphism and melt processes than previous snow schemes. To the best of our knowledge, this is the first time a snow-physics scheme of this level of complexity has been integrated into a global sea-ice model.

Here, we present the SI³+ISBA-ES model, the developments made to allow the integration of ISBA-ES within the SI³ framework and the validation of our coupled model in a unidimensional context focusing on the thermodynamic processes only (i.e: without representing the effects of sea-ice drift). To achieve this, we decided to validate our model using lagrangian data from the Surface Heat Budget of the Arctic Ocean (SHEBA) experiment (Perovich et al., 1999), where there are no direct effects of sea ice drift on snow properties, and against SnowModel-LG (Stroeve et al., 2020) data.

https://doi.org/10.5194/egusphere-2024-3220
Preprint. Discussion started: 4 February 2025

2 Materials & method

2.1 Sea-ice model

The sea-ice model used is SI³ (Sea Ice modeling Integrated Initiative, Vancoppenolle et al., 2023) and part of the Nucleus for European Modelling of the Ocean (NEMO, NEMO system team, 2022) in its version 4.2.2 . The core of SI³ integrates a suite of physical processes crucial for accurately simulating sea-ice evolution. These processes include thermodynamics, where heat exchanges between the atmosphere, ocean, and ice drive ice growth and melt. Additionally, SI³ accounts for mechanical forces such as ice deformation and ridging, which significantly impact ice thickness distribution and overall sea-ice morphology. The sea-ice thermodynamics is modeled using a 1D scheme that conserves energy (Bitz and Lipscomb, 1999), and includes a time-dependent salinity profile (Vancoppenolle et al., 2009). SI³ resolves a subgrid-scale sea-ice thickness distribution (Bitz et al., 2001; Thorndike et al., 1975). As the paper focuses on thermodynamics, we use the SI³ model in 1D (vertical) configurations, with only one sea-ice category and two ice layers, assuming that the dynamical processes affecting the snow and sea ice such as the ice deformation and ridging are negligible and that the advection is accounted by following the trajectory of the observations used to validate the model (see sec 2.4). Since we focus on the period where the snow is present, we neglect melt ponds over sea-ice in our configurations.

The surface forcing is computed by the NEMO bulk algorithm NCAR (Large and Yeager, 2004). turbulent heat fluxes over sea-ice are computed from 2m temperature and humidity, 10m winds and surface pressure. We assume that the snow covers the whole mesh in the presence of snow.

2.2 Snow model

The original version of the SI³ model used for this paper, prior to any snow model implementation, already simulates the snow cover assuming constant density (330 kg/m3) and thermal conductivity (0.31 W/m/K), no liquid water stored in snow and no snow metamorphism. When SI³ is hereafter coupled with the ISBA-ES snow model (see sec. 2), the snow cover is simply computed by ISBA-ES instead of the original SI³ trivial snow scheme.

The ISBA-Explicit Snow (ISBA-ES) snow model (Interactions between Soil Biosphere Atmosphere- Explicit Snow) developed by Boone and Etchevers (2001) and revised by Decharme et al. (2016) (see also the user manual, Boone, 2002). Initially developed for alpine conditions, it incorporates detailed representations of snowpack properties such as density, grain size, and thermal conductivity, and accounts for complex processes like snow accumulation, compaction, metamorphism and melt processes. The model is based on similar schemes as described by Kondo and Yamazaki (1990), Loth et al. (1993), Lynch-Stieglitz (1994) and Sun et al. (1999). We use 12 snow layers for our simulations. The number of vertical layers is fixed but their thickness is adapted at each time step to the total snow thickness, and the ISBA-ES prognostic variables are remapped at each time step on the ISBA-ES grid. At each time step, the snow layer thickness is updated to match the total snow thickness. The upper layer thickness is bounded so that its thickness does not exceed 0.2m (see Boone and Etchevers, 2001). Thickening

https://doi.org/10.5194/egusphere-2024-3220
Preprint. Discussion started: 4 February 2025

beyond that threshold ultimately results in snow transfer toward the layer below. The prognostic variables of the model are the snow heat content, the snow density, the snow thickness and the snow albedo. ISBA-ES includes parameterizations for processes like snow sublimation, blowing snow transport, or snowfall density enabling a comprehensive understanding of the physical mechanisms driving snowpack evolution. The snow metamorphism is not explicitly computed but is accounted for in the density and albedo parameterization through additional terms.

2.2.1 Snow density

The local rate of change of snow density ρ_s is parametrized after Brun et al. (1989, 1997):

$$\frac{\partial \rho_s}{\partial t} = \frac{\sigma_s}{\eta_s(T_s, \rho_s)} + \xi_{wind} \quad (1)$$

The first term on the right-hand side represents the snow overburden (the compactive viscosity term). It accounts for the pressure of the snow above (σs, in Pa) and its viscosity (ηs, in Pa s), determined by snow temperature and density (Kojima, 1967; Mellor, 1964). The second term ξ_{wind} represent the effect of the wind compaction (see 2.2.3).

2.2.2 Energy balance and heat flow

The heat content Hs (in $J.m^{-2}$) or energy needed to melt each snow layer is defined using an expression similar to those of Lynch-Stieglitz (1994) and Sun et al. (1999) as:

$$H_s = c_s h_s (T_s - T_f) - L_f (W_s - W_l) \quad (2)$$

Where h_s is the snow thickness, L_f is the latent heat of fusion, c_s is the snow heat capacity, defined following Versegy (1991), W_s is the Snow Water Equivalent (SWE) and W_l is the snow liquid water content. The heat content is used to diagnose the snow temperature using the equation above assuming that there is no liquid water in the snow layer ($W_l = 0$).

$$T_s = T_f + \frac{H_s + L_f W_s}{c_s h_s} \quad (3)$$

If the calculated temperature exceeds the freezing point, it is set to Tf, and the liquid water content is determined from the heat content equation as follows:

$$W_l = W_s + \frac{H_s}{L_f} \quad (4)$$

The layer-averaged snow temperature equation ($T_{s,k}$) for the snow layer k is then expressed as:

https://doi.org/10.5194/egusphere-2024-3220
Preprint. Discussion started: 4 February 2025

$$c_{s,k}D_{s,k}\frac{\partial T_{s,k}}{\partial t} = G_{s,k-1} - G_{s,k} - F_{s,k} \quad (5)$$

where F_s represents latent heat absorption or release due to phase changes (between water and ice). The heat flux G_s is simply expressed as:

$$G_s = J_s + Q_s \quad (6)$$

where Js and Qs are the heat conduction and radiation fluxes respectively. Qs is computed as follows:

$$Q_{s,i} = R_g(1-\alpha)\exp\left(-\nu_{s,k}h_{s,k}\right)k_s \quad (7)$$

Where R_g is the incoming shortwave radiation at the snow surface, α is the albedo and $\nu_{s,k}$ is the shortwave radiation extinction coefficient (Bohren and Barkstrom 1974). The extinction coefficient is computed as in Anderson (1976) and depends on the grain size, which is diagnosed from the snow layer density. The snow grain size is itself parametrized after Anderson (1976) and depends on the snow density. The snow albedo is modelled using the same decrease and increase rate formulations as Douville et al. (1995). The conduction flux Js is computed as follows:

$$J_{s,i} = \frac{2k_{s,k}\left(T_{s,k} - T_{s,k+1}\right)}{h_{s,k} + h_{s,k+1}} \quad (8)$$

Where $h_{s,k}$ is the snow layer thickness, and k_s is the snow thermal conductivity. Finally, the net heat flux $G_{s,0}$ at the atmosphere / snow interface is expressed as:

$$G_{s,0} = R_g(1-\alpha) + \varepsilon_n R_{at} - \sigma T_{s,1}^4 - H - LE + P_{rncw}\left(T_{al} - T_f\right) \quad (9)$$

Where ε_n is the snow emissivity (assumed to be 1), R_{at} is the downwelling atmospheric longwave radiation, σ is the Stefan-Botzmann constant, H and LE are the sensible and latent heat fluxes. The last term on the right-hand side of the equation above is a precipitation advection term where c_w represents the specific heat of water, P_{rn} is the rainfall rate, T_{al} is the temperature of rainfall, assumed to be the air temperature if it is above the temperature of fusion T_f.

2.2.3 Parametrizations

ISBA-ES uses parameterizations to represent various processes, including the changes in snow albedo, grain size, radiation extinction coefficient, compactive viscosity (that represent the snow overburden), thermal conductivity, snowfall density, and snow compaction due to wind (see sec 2.2.1 and 2.2.2). For the purposes of this study, some of the parameterizations were adjusted to better suit polar conditions. Thus, this section only outlines the parameterizations that differ from the standard ISBA-ES configuration as described by Decharme et al. (2016). Detailed descriptions of the parameterizations that remained unchanged from the default ISBA-ES configuration for this study are available in Boone and Etchevers (2001) and Decharme et al. (2016).

https://doi.org/10.5194/egusphere-2024-3220
Preprint. Discussion started: 4 February 2025

- *Snowfall density*

The density of the snow precipitation is parameterized as in Pahaut (1975):

$$\rho_{new} = A_{sn} + B_{sn}(T_a - T_f) + C_{sn}(V_a)^{1/2} \quad (10)$$

Where T_a is the air temperature, T_f is the temperature of fusion and V_a is the 10m wind speed. A_{sn}, B_{sn}, and C_{sn} are coefficients given by Pahaut (1975). Additionally, we tested another set of values for these coefficients, supposedly more suitable to the Arctic region given by Royer et al. (2021). The values of the coefficients are listed in table 1.

Coefficient	**A_{sn} ($kg.m^{-3}$)**	**B_{sn} ($m^{-3}.K^{-1}$)**	**C_{sn} ($m^{-7/2}.s^{1/2}$)**	**ρ_{max}**
Pahaut (1975)	*109*	*6*	*26*	*350*
Royer et al. (2021)	*109*	*6*	*59*	*600*

Table 1: Coefficients used for the parametrization of the snowfall density

- *Wind compaction*

The snowpack density is increased by the wind compaction processes. In ISBA-ES, the snowdrift ξ_{wind} (i.e: the wind compaction) is computed as:

$$\xi_{wind} = \frac{\partial \rho_{s,k}}{\partial t} = \frac{\rho_{max} - \rho_{s,k}}{\tau_i} \quad (11)$$

Where k denotes the snow layer, ρ_{max} is a maximum snow density authorized, and τ_i is the time characteristic for snow grain change under wind transport and is computed as:

$$\tau_k = \frac{\tau}{\mathrm{Wind}_{\mathrm{Effect}}\,\Gamma_{k,\mathrm{drift}}} \quad (12)$$

Where τ is empirically set to 48 h, $\mathrm{Wind}_{\mathrm{Effect}}$ is an empirical coefficient on wind effect, and ${}_t\Gamma_{i,drift}$ represents the grain driftability with an exponential decay function of the depth of the snow layer. In our experiments, we use two sets of values for the parameters ρ_{max} and $\mathrm{Wind}_{\mathrm{Effect}}$. The first one is the default parameters used in ISBA-ES, defined by Brun et al. (1997), where ρ_{max}=350 g/m3 and $\mathrm{Wind}_{\mathrm{Effect}}$=1 and the second one is the parameters defined by Royer et al. (2021), where ρ_{max}=600 g/m3 and $\mathrm{Wind}_{\mathrm{Effect}}$=1.5 which should be more suited to the Arctic region.

https://doi.org/10.5194/egusphere-2024-3220
Preprint. Discussion started: 4 February 2025

- *Thermal conductivity*

In the default version of ISBA-ES, the thermal conductivity is computed as in Anderson (1976). However, this parametrization may not be suited to the Arctic region. Thus, we implemented the Sturm et al. (1997) parametrization for the thermal conductivity, which is computed as follows:

$$k_s = 0.138 - 1.01\rho + 3.233\rho^2 \quad \{0.156 \leq \rho \leq 0.6\} \tag{13.a}$$

and

$$k_s = 0.023 + 0.234\rho \quad \{\rho \leq 0.156\} \tag{13.b}$$

2.2.4 Snow-ice formation

The ISBA-ES model was originally intended to model snow on land surface (SURFEX, Le Moigne et al., 2020) and thus does not account for snow / sea-ice coupling mechanisms such as the formation of snow-ice. Since we aim at modifying as little as possible the ISBA-ES code (see sec 2.3), sea-ice related snow processes (unresolved within ISBA-ES, which was developed for continental snow) are still treated by SI³ in the current SI³+ISBA-ES version of the code. However, the initial SI³ code intended for snow-ice formation was developed under the assumption of a constant snow density and a substantial rewrite of the code was necessary to account for the varying density within ISBA-ES. The method is similar to the one from Fichefet and Maqueda (1997), but accounting for a varying density over the vertical. We compute the snow / sea-ice thickness change Δh_{sni} assuming a zero freeboard as:

$$\Delta h_{sni} = \frac{\sum^k \rho_{s,k} h_{s,k} - (\rho_w - \rho_i) h_i}{\frac{\sum^k \rho_{s,k} h_{s,k}}{\sum^k h_{s,k}} + \rho_w - \rho_i} \tag{14}$$

Where ρ_s^k is the snow density and h_s^k is the snow thickness of the snow layer k, ρ_w is the density of seawater and ρ_i and h_i are the density and the thickness of the sea-ice respectively. Then, we iterate over the snow layers, starting from the bottom, to remove the mass $M_s = \sum_0^{\Delta h_{sni}} \rho_{s,k} h_{s,k}$, where $h_{s,k}$ is the thickness of each snow layer k and enthalpy E_s (in J/m²) $E_s = \sum_0^{\Delta h_{sni}} e_{s,k} h_{s,k}$ where $e_{s,k}$ is the enthalpy in J/m³ of each snow layer from the snow due to the thickness change.

Assuming that the snow-ice has the same density as the sea-ice (constant in SI³), the mass change for the sea ice is computed as $M_i = \rho_i \Delta h_{sni}$. The salinity change associated with the snow-ice formation is computed as:

$$dS_i = \frac{S_{oce}(\rho_i \Delta h_{sni} - M_s)}{\rho_i - S_i \Delta h_{sni}} \times \frac{1}{h_i} \tag{15}$$

Where S_{oce} and S_i are the salinities of seawater and ice respectively and the new snow-ice enthalpy $E_{i,sni}$ (in J/m²) added to the upper layer of sea-ice is computed as:

$$E_{i,sni} = E_s + (M_s - \rho_i \Delta h_{sni}) E_w \tag{16}$$

https://doi.org/10.5194/egusphere-2024-3220
Preprint. Discussion started: 4 February 2025

where E_w is the enthalpy of seawater.

2.3 Snow and ice coupling

In this work, we couple the ISBA-ES model to the SI³ model so that most snow thermodynamic processes are not computed anymore by the original SI³ snow scheme but by ISBA-ES. However, some sea-ice related processes (not accounted for in the ISBA-ES original model) such as the snow-ice formation are not resolved by the current version of ISBA-ES and are still resolved within the sea-ice model. The coupling is made online, meaning that the ISBA-ES code is incorporated within SI³ and no coupler is needed. However, in the present version of the code the interaction of the snow with the sea-ice dynamics and with the melt ponds are not yet implemented so we focus on evaluating the thermodynamic part of the coupling.

At the beginning of a time step, the lower boundary condition of ISBA-ES is given by the temperature and the thermal conductivity of the upper sea-ice layer. After the resolution of snow processes, the conduction flux at the snow-ice interface computed by ISBA-ES is sent to SI³ and is used as upper boundary condition for the temperature solving in the sea-ice. Note that since the snow-ice conversion is computed within SI³ and not ISBA-ES, the vertical profiles of the ISBA-ES prognostic variables are also exchanged between the two models and updated in both ISBA-ES (due to "snow-only" processes) and SI³ (due to snow-ice conversion).

The conduction flux at the snow-ice interface Fc is recomputed in ISBA-ES as $F_c = -K_{s-i} \cdot \left(T_{i,1} - T_{s,N}\right)$, where T is the temperature, the subscripts i and sn denote the ice or the snow and the index 1, N denotes the upper layer and the lower layer respectively. Ks-i is the thermal conductivity at the snow-ice interface, which is computed as in SI³ and Vancoppenolle et al. (2012): $K_{s-i} = \frac{(h_{s,N}+h_{i,0})\cdot(k_{i,0}\cdot k_{s,N})}{(k_{i,0}\cdot h_{s,N}+k_s\cdot h_{i,0})}$ where k is the thermal conductivity and h is the thickness of the corresponding layer (depending on the subscript).

The ISBA-ES model is called just before the resolution of the sea ice thermodynamic processes. The basic iteration procedure for the SI³+ISBA-ES model follows the steps below:

- The ISBA-ES model is called. The model reads its prognostic variables (snow thickness, density, heat content and albedo) from a restart or from previous time step and the temperature and conductivity of the first sea-ice layer from current time step. Then, it computes the changes in snow thickness, heat content and density due to snowfall and remaps the prognostic variables on its vertical grid. Then, the model resolves the evolution of prognostic variables accounting for processes such as settling, compaction, metamorphism, and melting. Additionally, it calculates the conduction flux at the interface between the snow and sea ice, and the radiative flux transferred to the sea-ice below. At the end of the ISBA-ES iteration, the vertical profiles of ISBA-ES prognostic variables along with any remaining heat and evaporation flux to be transmitted to SI³ (if all snow has melted during a time step) are stored.

https://doi.org/10.5194/egusphere-2024-3220
Preprint. Discussion started: 4 February 2025

- The conduction flux at the interface between the snow and the sea-ice estimated by ISBA-ES is then used as a boundary condition to solve the temperature equation in the sea-ice by SI³, and changes in ice thickness due to ice melt are computed by SI³ as well.
- If the snow exceeds a certain thickness and density so that the snow base is pushed below the freeboard, snow-ice formation occurs, and the vertical profiles of snow and sea-ice thickness and enthalpy are updated and saved for use in the next time step.

2.4 Validation data

We use the data collected during the Surface Heat Budget of the Arctic Ocean (SHEBA) experiment to validate our model (Perovich et al., 1999). The SHEBA experiment took place from 1997 to 1998. During this period, several snow variables useful to validate our model such as the snow thickness, the snow surface temperature and the snow-ice interface temperature were collected daily. Snow thicknesses were gathered by employing magnoprobes and ruler measurements along transects ranging from 200 to 500 meters in length. We used the same SHEBA snow thickness dataset as Stroeve et al. (2020), where in-situ observations were aggregated over all transects and averaged for each day. Additionally, the snow surface temperature and the snow-ice interface temperature were collected from thermistors as described in Persson et al. (2002).

We also compared our model with the outputs of the SnowModel-LG simulations performed by Liston et al. (2020) and Stroeve et al. (2020). SnowModel-LG is a multilayer model specifically designed to simulate the key physical processes governing the seasonal evolution of snow thickness and density over sea ice. It operates on a Lagrangian framework and incorporates various parameterizations to account for processes like blowing snow redistribution, sublimation, changes in density and grain size, and snow metamorphism. More details about the model can be found in by Liston et al. (2020) and Stroeve et al. (2020). The model is forced either by NASA's Modern Era Retrospective-Analysis for Research and Applications-Version 2 (MERRA-2, Gelaro et al., 2017) or by the European Centre for Medium-Range Weather Forecasts (ECMWF) atmospheric data (ERA5, Hersbach et al., 2020). Approximately 61,000 lagrangian parcels were simulated with this model over the Arctic, covering the 1980 – 2018 period. We also use the SnowModel-LG data described in Stroeve et al. (2020), which gives an estimate of the classic behavior of a snow model of an intermediate complexity. To compare SnowModel-LG with our simulations over the SHEBA site, we used the same lagrangian parcel used in Stroeve et al. (2020) which is a representative parcel located initially near the departure location of the SHEBA campaign (see sec. 3.1 in their paper). The path of the SHEBA experiment is illustrated in Figure 1.

We also set-up an additional model-only configuration in the Arctic marginal zone to illustrate the effect of the snow-ice conversion parametrization on the snow-ice system. The point selected for this configuration is represented by a red cross in Figure 1.

https://doi.org/10.5194/egusphere-2024-3220
Preprint. Discussion started: 4 February 2025

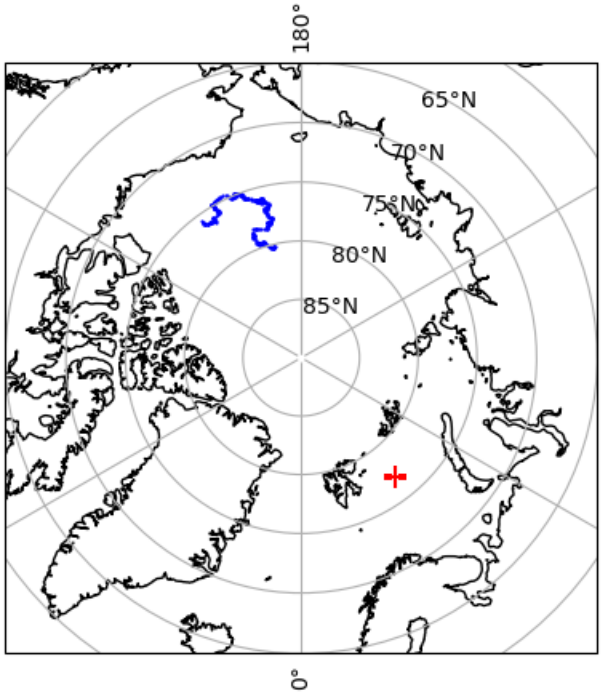

Figure 1: Trajectory of the SHEBA experiment during the observation period (blue) and location of the configuration in the Arctic marginal ice zone (red cross).

2.5 Configurations

Among all the parameterizations available in ISBA-ES, the parameterizations of the snowfall density and of the wind-induced compaction are the ones with the greatest impact on the snow thickness and density. Thus, we performed a set of experiments to evaluate the sensitivity of the model to these parameterizations. Two experiments, P76 and R21 using the Pahaut (1975) and Royer et al. (2021) coefficients (see sec. 2.2.3) for the parametrization for the snowfall density respectively were conducted without the snowdrift parameterizations active. Additionally, two similar experiments, P76_DRIFT and R21_DRIFT, were conducted with the snowdrift parameterization enabled, using the Pahaut (1975) and Royer et al. (2021) coefficients, respectively, for snowfall density parametrization. Another experiment, named R21_DRIFT21, was set up using the Royer et al. (2021) coefficients for both snowfall density and snowdrift parametrization (see sec. 2.2.3). Lastly, we prepared a configuration called SI3, where the snowpack is simulated by SI³ in its NEMO 4.2 stable version (i.e., without ISBA-ES), to examine the differences in snow state simulation between SI³-only and SI³+ISBA-ES. The parameterizations used in these experiments are summarized in Table 2.

SI³ is used in sea-ice only mode, meaning that the sea-ice / snow component is forced from both oceanic and atmospheric sides. We use the GLORYS12 (Lellouche et al., 2018) reanalysis as forcing data for the ocean and either the MERRA2 or

https://doi.org/10.5194/egusphere-2024-3220
Preprint. Discussion started: 4 February 2025

ERA5 reanalysis for the atmosphere (more information is provided in the results section. To force our simulations, we followed the trajectory of the SHEBA tower and extracted the forcing data at the position of the tower for each day.

The simulations were initialized on the 3rd of november 1997. We use the SHEBA snow thickness averaged over all snow transects for this date (0.153 m) as initial value for our model. We also use the SnowModel-LG density for this date (191 kg/m³) to initialize ISBA-ES simulations. Note that because of this, the ISBA-ES simulations are initialized with the same thickness as the SI3-only simulation but with a different mass per unit area (0.153 m x 191 kg/m³ = 29.2 kg/m²) than the SI3-only simulation which use a constant density (0.153 m x 191 kg/m³ = 50.5 kg/m²). For the sea-ice thickness and concentration, we use the GLORYS12 value for this date (2.95 m, 0.88 respectively).

Simulation name	Configuration	Snow compaction (due to overburden)	Snowfall density	Thermal conductivity	Metamorphism	Snowdrift (compaction by wind)	Albedo
SI3	SI³	Constant, 330 kg/m3	Constant, 330 kg/m3	Constant, 0.31 (W/m/K)	None	None	Constant, 0.83
P76	SI³ + ISBA-ES	Brun et al., (1989) and Vionnet et al. (2012)	Pahaut (1976)	Sturm et al., 2002	Parametrized in density & albedo formulations	None	Douville et al. (1995)
P76_DRIFT	SI³ + ISBA-ES	Brun et al., (1989) and Vionnet et al. (2012)	Pahaut (1976)	Sturm et al., 2002	Parametrized in density & albedo formulations	Brun et al. (1997)	Douville et al. (1995)
R21	SI³ + ISBA-ES	Brun et al., (1989) and Vionnet et al. (2012)	Royer et al. (2021)	Sturm et al., 2002	Parametrized in density & albedo formulations	None	Douville et al. (1995)
R21_DRIFT	SI³ + ISBA-ES	Brun et al., (1989) and Vionnet et al. (2012)	Royer et al. (2021)	Sturm et al., 2002	Parametrized in density & albedo formulations	Brun et al. (1997)	Douville et al. (1995)
R21_DRIFT21	SI³ + ISBA-ES	Brun et al., (1989) and Vionnet et al. (2012)	Royer et al. (2021)	Sturm et al., 2002	Parametrized in density & albedo formulations	Royer et al. (2021)	Douville et al. (1995)

Table 2: Parameterizations used to represent snow processes in all SI³+ISBA-ES (and SI³-only) simulations.

https://doi.org/10.5194/egusphere-2024-3220
Preprint. Discussion started: 4 February 2025

3 Results

3.1 Validation at the SHEBA site

3.1.1 Sensitivity to the atmospheric forcing

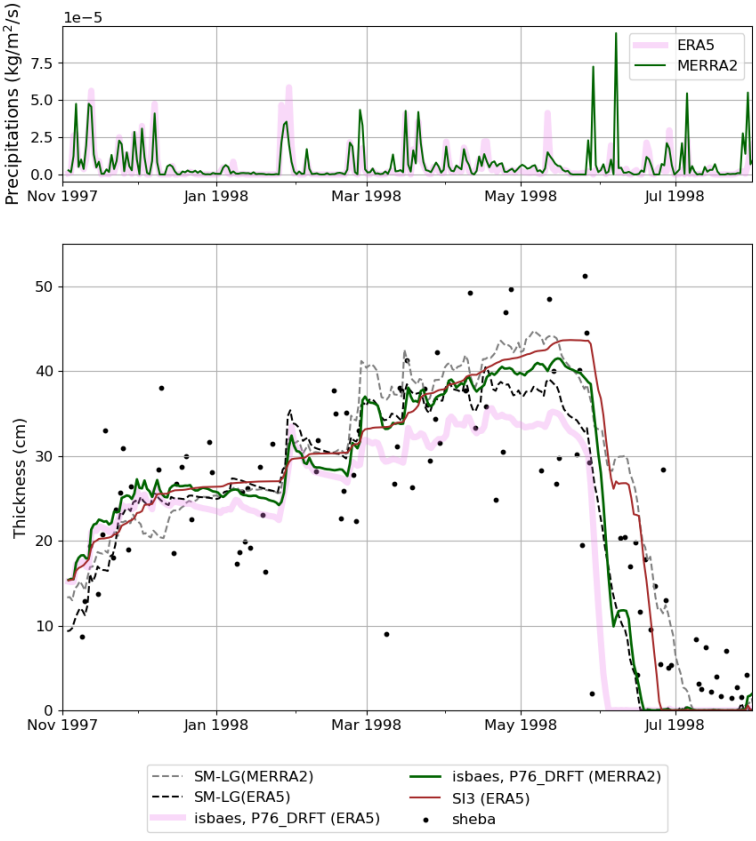

Figure 2: Top panel: snow precipitation (in kg/m3/s) in MERRA2 (thin green line) and ERA5 (large green line) forcings. Bottom panel: Observed (black dots) and simulated (lines) snow thickness at SHEBA during the November 1997 - September 1998 period. The observations were aggregated over all transects (Perovich et al. 1999). The large pink line and the thin green line represent the snow thickness for a simulation using the P76_DRIFT configuration using ERA5 and MERRA2 as forcing respectively. The dotted lines represent the snow thickness from the SnowModel-LG product.

Following Stroeve et al. (2021), we first investigate the effect of the atmospheric forcing on the snowpack variability. For this, we conducted two simulations using the P76_DRIFT setup, varying only in the atmospheric forcing applied - either ERA5 or MERRA2 - over the duration of the SHEBA experiment (Perovich et al., 1999), following the tower trajectory. We compare the results obtained from our simulations with the SHEBA data, and with the outputs available from the SnowModel-LG simulations from Liston et al. (2020) and Stroeve et al. (2020). While the resolution disparity between our model's estimates (roughly equivalent to the resolution of the forcing, 31km for ERA5) and the point measurements at SHEBA prevents a quantitative assessment of our simulations, it does provide an estimate of the simulation's realism.

https://doi.org/10.5194/egusphere-2024-3220
Preprint. Discussion started: 4 February 2025

Overall, the snow thickness computed by ISBA-ES with the P76_DRIFT configuration compares well with the SHEBA observations and SnowModel-LG outputs (Figure 2). When using ERA5 as the atmospheric forcing, snow thickness is slightly underestimated by an average of 3.5 cm over the period. In contrast, a better match with observations is achieved using MERRA2, with the underestimation reduced to an average of 0.5 cm (refer to the scores in Table 3). In particular, the snow melt is delayed in comparison to the ERA5 simulation because MERRA2 reports more precipitation than ERA5 during the melt season (from May to August). During the SHEBA period, switching the atmospheric forcing from ERA5 to MERRA2 results in an average change in snow thickness of approximately 3.2 cm in ISBA-ES simulations. This difference aligns with SnowModel-LG outputs, where the change in atmospheric forcing leads to an average change in snow thickness of around 3.1 cm.

The temporal variability of SI³ + ISBA-ES simulations align more closely with the SnowModel-LG outputs compared to the SI³-only simulation, where the snow thickness varies less over time. This is because SI³ + ISBA-ES simulates the temporal evolution of precipitation density, making it more responsive to changes in atmospheric temperature and wind compared to the SI³-only simulation in which the density of the snowfall is constant.

Simulation	Mean (cm)	Mean difference with observations (cm)	Mean RMSE with observations (cm)	R2 (with observations)
P76_DRIFT (ERA5)	21.7	-3.4	7.0	0.79
P76_DRIFT (MERRA2)	24.9	-0.5	6.7	0.79
SI³ (MERRA2)	26.4	1.4	6.7	0.78

Table 3: Averaged scores obtained for the snow thickness (cm) during the November 1997 to August 1998 period for the sensitivity tests on the atmospheric forcing.

https://doi.org/10.5194/egusphere-2024-3220
Preprint. Discussion started: 4 February 2025

3.1.2 Sensitivity to the parametrization of snowfall density and snowdrift

This section focuses on analysing the effects of parameterizations for snowfall density and wind-driven snow compaction (snowdrift). Given that a better agreement with the observations was achieved using MERRA2 as atmospheric forcing, we have decided to use this forcing for our simulations. Therefore, the MERRA2 reanalysis is used to force all simulations presented in the following.

We performed six simulations with the P76, P76_DRIFT, R21, R21_DRIFT, R21_DRIFT21 and SI3 configurations over the period and the path of the SHEBA experiment (Perovich et al., 1999) as it is described in the previous section.

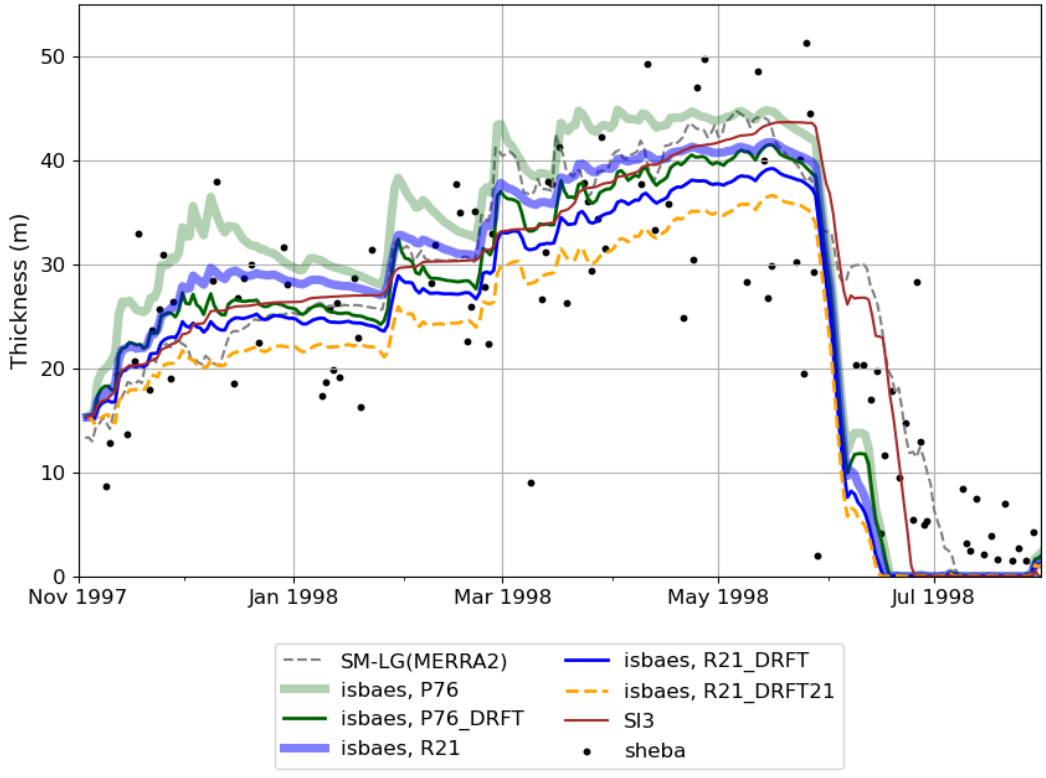

Figure 3: Observed (black dots) and simulated (lines) snow thickness at SHEBA during the November 1997 - September 1998 period. The observations were aggregated over all transects (Perovich et al. 1999).

https://doi.org/10.5194/egusphere-2024-3220
Preprint. Discussion started: 4 February 2025

Figure 3 depicts the aggregated snow thickness from all SHEBA transects compared to our simulations and to SnowModel-LG outputs. The scores obtained for each simulation are summarized in table 4. Overall, all simulations compare reasonably well with the measured snow thickness at SHEBA during the accumulation period. The best scores are nonetheless obtained for the P76_DRIFT simulation (see table 4). As expected, the snowdrift parametrization tends to reduce the snow thickness through snow compaction by ~3.9 cm (ISBAES_dlft - P76_DRIFT) in average over the period for the default parameters and by ~5.1 cm with the Royer et al. (2021) parameters for the snowdrift and the snowfall density (R21 - R21_DRIFT21). The choice of the parametrization for the snowfall density and for the snowdrift results in an average change in snow thickness of approximately 3.9 cm in ISBA-ES simulations (P76_DRIFT - IBAES_R21_DRIFT21), which is roughly the same order of magnitude than the thickness change associated with the choice of the atmospheric forcing (see sec. 3.1.1).

However, the snow tends to disappear in all simulations during the first month of the melting season while it persists until the end of the melting season (roughly, from May to August) in the observations. In the melt season (from May 1998), the excessively fast melting of the snow in all ISBA-ES simulations compared to the SHEBA observations and the SI³-only simulation is likely due to the ISBA-ES albedo parameterization which seems to underestimate the albedo during the melt season. Indeed, when the snow albedo is forced to 0.8 (which is higher than the albedo simulated with ISBA-ES, see Figure 8), the snow thickness matches the SnowModel-LG simulation during the melt period (see supporting material, Figure S1). This underestimation of the albedo is probably due to its dependency on the density, or to the density itself.

The SI³-only simulation more successfully reproduces the snow melt, resulting in thicker snow during this period. The improved performance of the SI³-only simulation during the melt season may be attributed to its use of a constant snow albedo (0.83, see Figure 8.) and/or the different initialization of snow mass in the SI³-only simulation compared to the ISBA-ES simulations (refer to section 2.e).

Note that the snow melts completely in summer in all simulations (including SnowModel-LG simulations) whereas snow remains in the observations, which also shows that the snow melt is likely to be overestimated by the models.

https://doi.org/10.5194/egusphere-2024-3220
Preprint. Discussion started: 4 February 2025

Simulation	Mean (cm)	Mean difference with observations (cm)	Mean RMSE with observations (cm)	R2 (with observations)
P76	28.8	3.1	8.0	0.78
P76_DRIFT	24.9	-0.5	6.7	0.79
R21	26.0	0.6	7.1	0.79
R21_DRIFT	23.2	-2.0	6.9	0.79
R21_DRIFT21	20.9	-4.0	7.3	0.78
SI3	26.4	1.4	6.7	0.78

Table 4: Averaged scores obtained for the snow thickness (cm) during the November 1997 to August 1998 period for the sensitivity tests on the snow density parametrizations.

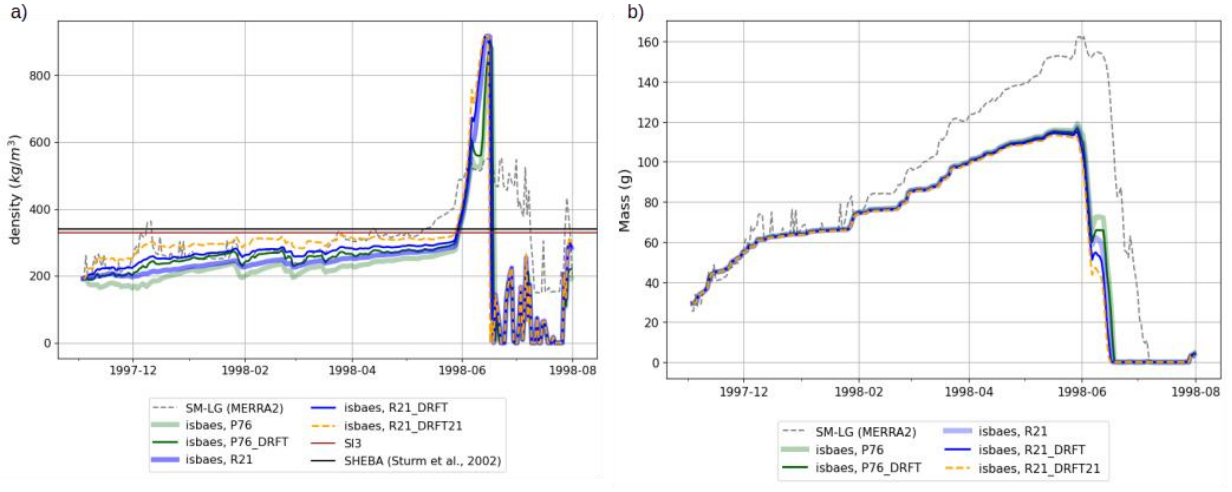

Figure 4: Snow density (a) and mass (b) at SHEBA during the November 1997 - September 1998 period.

https://doi.org/10.5194/egusphere-2024-3220
Preprint. Discussion started: 4 February 2025

The discrepancies in snow thickness between the different ISBA-ES simulations are related to the density of snow: a denser snow will be associated with a thinner snowpack and vice versa. The evolution of the density during the SHEBA period is represented in Figure 4.a. For the ISBA-ES simulations, the mean densities over this period are 225.6, 260.7, 244.6, 275.5 and 303.9 g/m3 for P76, P76_DRIFT, R21, R21_DRIFT and R21_DRIFT21 respectively, which is slightly lower with the average bulk density of 340g/m3 measured at SHEBA by Sturm et al.(2002), and with the mean densities of SnowModel_LG outputs (281.8 g/m3 when forced by MERRA2 and 263.0 when forced by ERA5). The better agreement with the SnowModel-LG depth-averaged density is found for the ISBA-ES simulations using the snowdrift parametrization (P76_DRIFT and R21_DRIFT).

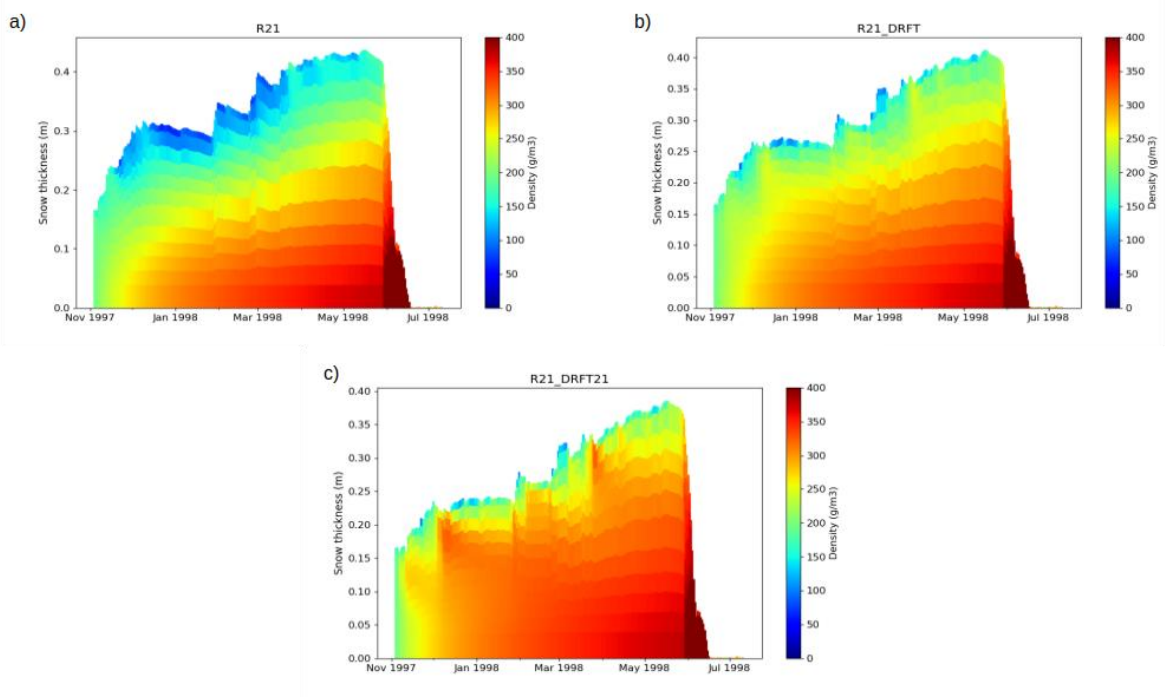

Figure 5: snow thickness and density (contours) for R21 (a), R21_DRIFT (b) and R21_DRIFT21 (c) at SHEBA during the November 1997 - June 1998 period.

Over the arctic region, the snowpack typically consists of a basal depth hoar (low-density, brittle, highly permeable type of snow) overlaid by a hard and dense wind slab (e.g: Domine et al., 2018; Sturm et al., 2002, and references therein). Without the snowdrift parameterization activated, the snowpack is not compacted near the surface (Figure 5.a). Consequently, the P76 and R21 simulations fail to represent the typical Arctic wind slab layer. Alternatively, the default ISBA-ES snowdrift parameterization (Brun et al., 1997) tends to increase near-surface density (Figure 5.b). However, the maximum density in the

https://doi.org/10.5194/egusphere-2024-3220
Preprint. Discussion started: 4 February 2025

Brun et al. (1997) snowdrift parameterization is 350 g/m³, which is lower than the mean density of the wind slab layers found at SHEBA in Sturm et al. (2002) (403 g/m³). Therefore, the P76_DRIFT and R21_DRIFT simulations still lack an accurate representation of the wind slabs. In contrast, the Royer et al. (2021) parameterization allows for higher densities and yields significantly different results (Figure 5.c). During winter, R21_DRIFT21 simulates higher densities near the snowpack surface, which could be attributed to a wind slab layer. Thus, although R21_DRIFT21 appears to overestimate the mean density, likely due to an inaccurate representation of the depth hoar layer, it does allow for a more realistic representation of wind slab layers in the Arctic region. In SI3, the density is constant and equal to 330 g/m3. The snow mass (Figure 4.b) remains unaffected by the choice of the parametrization for snowfall density and/or wind-induced compaction in the accumulation period. In the melt season however, the melt rates are affected by the difference in heat diffusion associated with the differences in thermal conductivity.

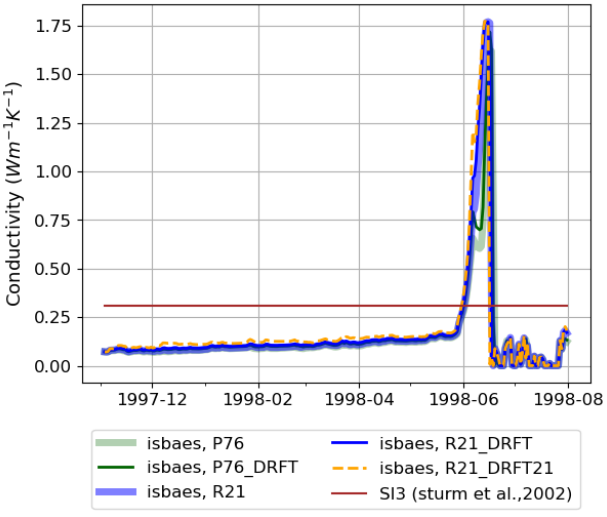

Figure 6: Snow conductivity at SHEBA during the November 1997 - September 1998 period.

Indeed, the snow density drives its thermal conductivity and thus the heat transfer within the snowpack. In SI³, it is a fixed parameter at 0.31 W/m/K but in ISBA-ES, which is the value measured at SHEBA by Sturm et al. (2002), it can evolve as a function of the density. Figure 6 represents the time series of the snow thermal conductivity for SI³ only and SI³+ISBAES simulations. The snowpack bulk conductivity from December 1997 to April 1998 is 0.10 W/m/K for the simulations without the snowdrift parametrization, 0.11 W/m/K for the simulations using the Brun et al. (1997) snowdrift parametrization and 0.14 W/m/K with the Royer et al. (2021) snowdrift parameters. Those conductivity estimates are consistent with the measured bulk conductivity at SHEBA (0.14 W/m/K) but lower than the estimate inferred from ice growth and temperature gradients (0.31 W/m/K) during the winter season (see Sturm et al., 2002).

https://doi.org/10.5194/egusphere-2024-3220
Preprint. Discussion started: 4 February 2025

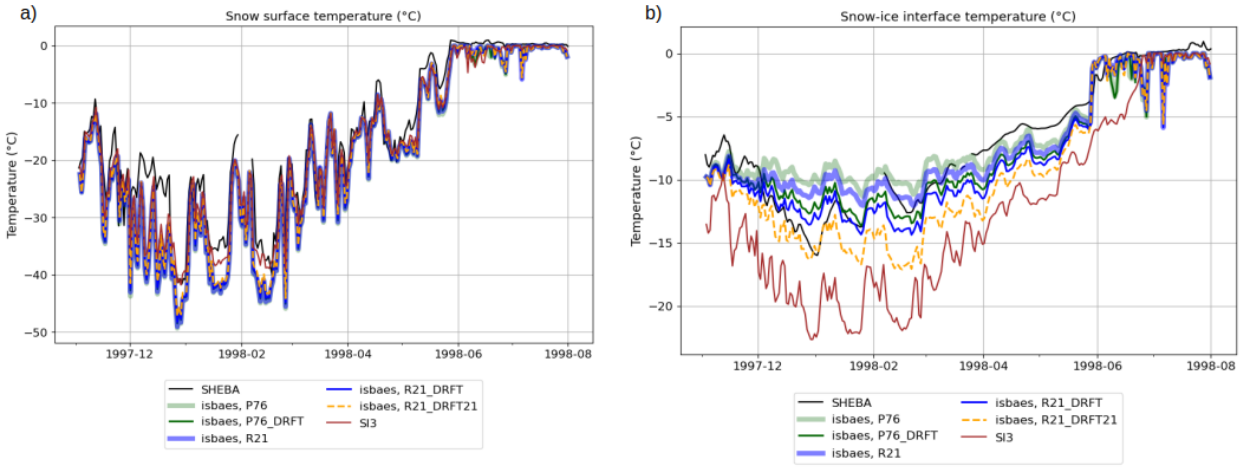

Figure 7: Measured and simulated snow surface (a) and snow-ice interface (b) temperatures (°C) at SHEBA during the November 1997 - September 1998 period.

435

The thermal conductivity drives the heat transfer through the snowpack. The snow surface temperature and the snow-ice interface temperature were measured at the SHEBA tower during the whole SHEBA period. Figure 7 represents the measured and simulated snow temperatures at both the snow surface and at the sea-ice interface. Note that the snow temperatures were not available in the SnowModel-LG outputs. The snow surface temperature is strongly dependent on the atmospheric forcing, and all SI³+ISBA-ES or SI³-only simulations compare well with the observations and simulate a snow surface temperature consistent with the observations and a realistic temporal variability. All SI³+ISBA-ES simulations simulate a snow-ice interfacial temperature more consistent with the observations than SI³-only simulation. Thus, this suggests that the thermal conductivity simulated by ISBA-ES is more realistic than the mean value used in SI³. Note that the best agreement with the observations is found for the P76_DRIFT simulation. The lowest interfacial temperatures simulated by the SI³ + ISBA-ES simulations range from ~-12°C for P76 to ~-18°C for R21_DRIFT21 simulation. Note that this range depends on the parametrization used for the computation of the snow thermal conductivity, as we found a bigger range of temperatures with the Anderson (1976) parametrization (used in the ISBA-ES default version) (Not shown). In brief, these results highlight the sensitivity of the snowpack bottom temperature to the choice of the parametrization for the snowfall density and/or wind compaction, but also the importance of simulating the right bulk thermal conductivity in the snowpack as it will condition the sea-ice growth and melt below.

https://doi.org/10.5194/egusphere-2024-3220
Preprint. Discussion started: 4 February 2025

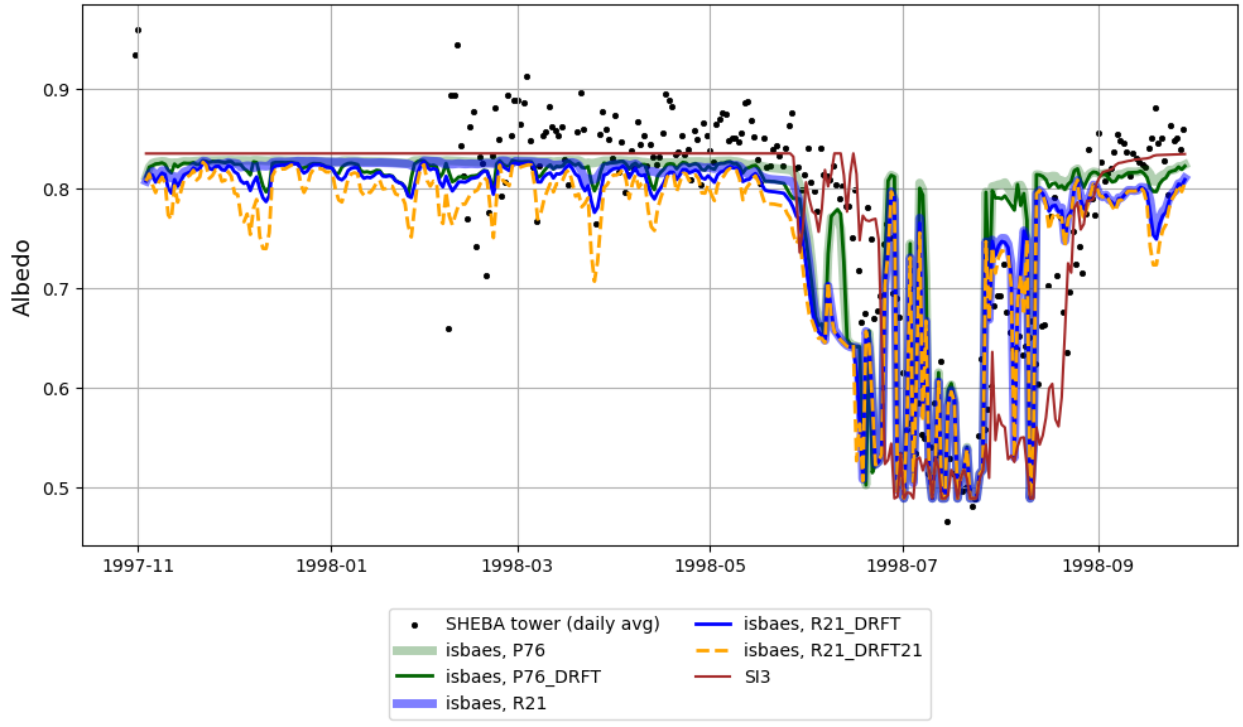

Figure 8: Daily averages of measured (dots) and simulated (lines) snow-ice albedo at the SHEBA tower during the November 1997 - September 1998 period.

455

The snow/ice albedo was also measured at the SHEBA tower during the melt season, and it is represented in figure 8 along with the albedo simulated by SI³+ISBA-ES and SI³-only simulations. In SI³, the snow albedo is fixed to 0.83 and is constant during the accumulation period, which is consistent with the observations at the SHEBA tower. In SI³+ISBA-ES simulations, the albedo varies with the snowpack density and thus it is sensitive to the choice of the parametrization for the snowfall density
460 and/or wind compaction. It is slightly lower than the albedo in SI³ as it is bounded to 0.83 and decreases when the density increases. P76 and R21 simulate a realistic albedo, but the other simulations underestimate the albedo. When the snow drift parametrization is active, the albedo fluctuates more as it depends on the density of the first layer which is very sensitive to the compaction by wind.

465

https://doi.org/10.5194/egusphere-2024-3220
Preprint. Discussion started: 4 February 2025

3.2 Snow-ice conversion

In some cases, the accumulated snow can exceed a certain thickness and density so that the snow base is pushed below the freeboard, leading to flooding of the snow base followed by a freezing of the slush layer and the formation of snow-ice (Jutras et al., 2016). Given the technical difficulties for sampling zones where the snow-ice formation is active, long-term records of data showing snow-ice formation do not exist yet to our knowledge. Thus, in this part, we only aim at illustrating the impact of the snow-ice parameterization on the ice and snow thicknesses in our model. To do this, we performed two simulations: one with the ISBAES_dlft configuration, with the snow-ice parametrization active (P76) and one where it is deactivated (P76_nosni), at a single location in the arctic sea-ice marginal zone (see the red cross in Fig 1), where the snow-ice conversion process plays an important role, during the January 1993 to June 1993 period, during which the snow-ice conversion was important. The simulations are forced by the ERA5 and GLORYS12 reanalyses and initiated with the snow thicknesses from SnowModel-LG and the sea-ice depths and concentration from GLORYS12.

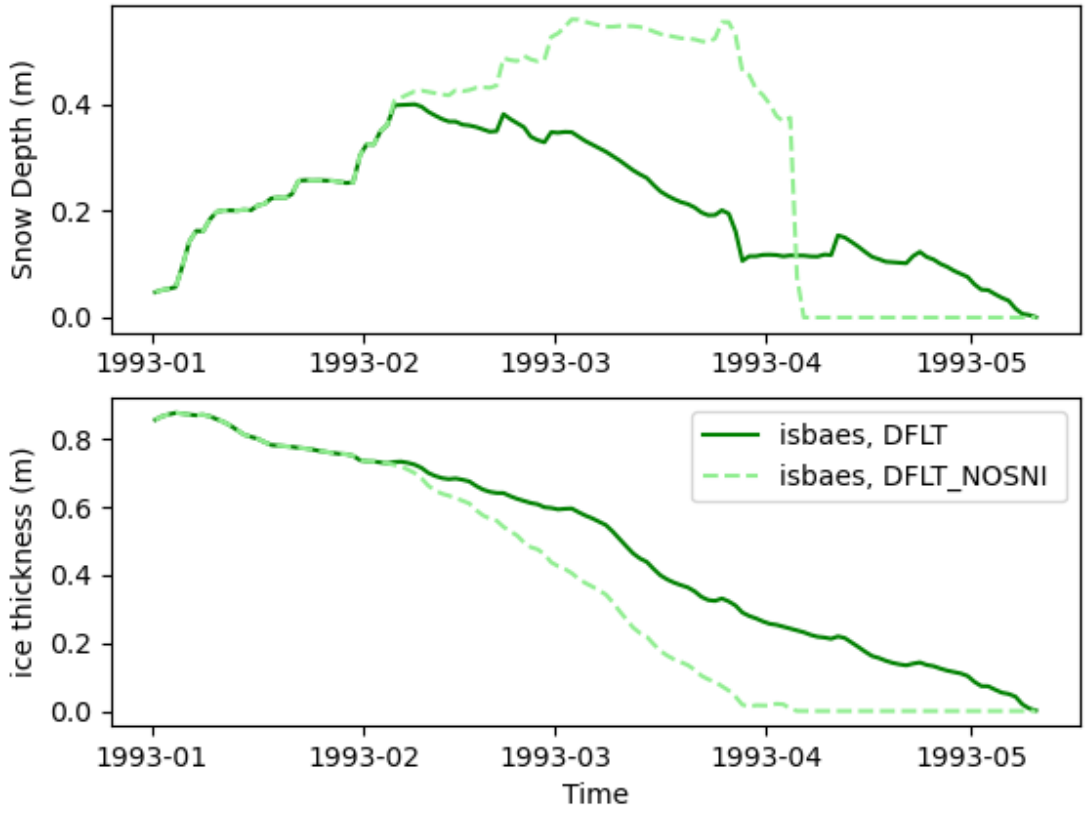

Figure 9: Simulated snow (top) and ice (bottom) thicknesses (m) for a configuration in t the arctic sea-ice marginal zone.

https://doi.org/10.5194/egusphere-2024-3220
Preprint. Discussion started: 4 February 2025

Figure 9 depicts the simulated snow and ice thicknesses for the P76 and P76_nosni simulations. At the location selected (see red cross in Fig 1), the snow accumulated until early April 1993 in P76_nosni. After this period, the snow thickness reduced to zero as the sea-ice below has melted completely. In P76, the snow accumulated until February 1993 only, then it started to decrease as a result of the snow-ice conversion. As the snow-ice conversion transforms snow into sea-ice, it delays the date where the sea-ice has completely melted from early April to early May 1993. This suggests that the snow ice conversion can play an important role in certain areas of arctic sea-ice marginal zones.

4 Discussion / conclusion

Here we implemented for the first time a detailed snow-physics scheme (ISBA-ES) into a sea-ice model (SI³), which serves as the sea-ice component for upcoming versions of the CNRM-CM climate model. The ISBA-ES snow model incorporates detailed representations of snowpack properties such as density, grain size, and thermal conductivity, allowing for more accurate simulation of snow accumulation, compaction, metamorphism and melt processes than usual slab models (such as the original snow parameterization in SI³ that use a constant density and thermal conductivity). Its integration in SI³ does not use a coupler and the ISBA-ES code is compiled within the SI³ framework.

The integration of such a detailed snow model within a sea-ice model is, per se, a technical challenge. We integrated ISBA-ES to SI³ so that snow thermodynamic processes are not computed anymore by SI³ but by ISBA-ES. However, we aimed at modifying as little as possible the ISBA-ES model to facilitate the phasing with the future versions of the model. Thus, some sea-ice related processes (thus not resolved by this alpine snow model) such as the snow-ice formation are still resolved within the sea-ice model. At the snow-ice interface, transfer of heat from snow to ice is made through a heat conduction flux. The SI³+ISBA-ES model is currently fully functional in 1D without the sea-ice dynamics activated and conserves the heat, mass and salt.

The aim of this article was to present the first developments made to allow the integration of ISBA-ES into SI³ and the performance of the model, focusing on the thermodynamic processes only. Here, we validated the SI³+ISBA-ES model over 1D configurations following the path of the Heat Budget of the Arctic Ocean (SHEBA) experiment (Perovich et al., 1999). We performed several simulations using different parameterizations for computing the snowfall density and the compaction by wind to illustrate the sensitivity of our model to these parametrizations. We compared these simulations with the SHEBA observations and with the SnowModel-LG outputs from Stroeve et al., 2020, which is, to date, the most sophisticated and validated snow-on-sea-ice model available. Overall, our model simulates realistic snow thicknesses, densities and temperatures, compared to the SHEBA observations and SnowModel-LG outputs, and captures well the temporal variability of these variables. Compared to the previous snow scheme used in SI³ that assumes constant snow density and thermal conductivity, our model is able to realistically simulate the temporal evolution of the snow bulk density and thermal conductivity of the snowpack. As a result, the temperature at the snow-ice interface is more accurate with SI³+ISBAES

https://doi.org/10.5194/egusphere-2024-3220
Preprint. Discussion started: 4 February 2025

compared to the previous SI³ snow scheme, leading to a more realistic heat transfer to the underlying sea ice. This emphasizes the importance of modeling the temporal changes in the density and thermal conductivity of the snow layers on Arctic sea ice. In agreement with Lecomte et al. (2013), we demonstrated that snowpack thicknesses, densities, and conductivities are equally sensitive to the parametrization choices for computing snowfall density and representing snow compaction by wind, as well as to the choice of atmospheric forcing. Therefore, specific tuning of these ISBA-ES parameterizations is as crucial as having realistic forcing to accurately represent the snowpack over the Arctic. The best agreement with the SHEBA observations for snow thickness and temperature is achieved using the Brun et al. (1997) parameters for snowfall density and snow compaction (the default parameters of ISBA-ES). However, given 1. the significant spatial variability of Arctic snow cover, 2. the resolution disparity between model grid cell area estimates and point measurements at SHEBA, and 3. the uncertainties in observations, it is difficult to highlight the superiority of any SI³+ISBA-ES configuration over another. Nonetheless, our results highlight the realism of the SI³+ISBAES model, and the importance of the choice of such parametrizations.

We also demonstrated that the default maximum density according to Brun et al. (1997) for the snowdrift parameterization is insufficient for accurately capturing the upper wind slab layer typical of the Arctic region. Setting a higher maximum density as proposed by Royer et al. (2021) appears to better represent this wind slab layer, although it results in a slightly over-dense snowpack. However, the absence of long-term records of snow density profiles over sea ice complicates the tuning of wind compaction parameterizations. Future field studies collecting such data could significantly enhance the fidelity of density profiles in Arctic snow models.

In addition to refining the snow compaction or snowfall parameterizations, improving the density profile in ISBA-ES could also be achieved by incorporating a representation of water vapor fluxes within the snowpack. Indeed, the strong temperature gradients in the Arctic snowpack create gradients in saturation water vapor density and pressure, which result in diffusion (Sturm and Benson, 1997) that can significantly influence the snowpack's density profiles (Domine et al., 2016; Jafari and Lehning, 2023). SI³+ISBA-ES simulations could benefit from future studies that focus on implementing and testing the impact of representing water vapor fluxes within the snowpack on the simulated density profiles.

The model could be also further improved by incorporating specific snow-on-sea-ice processes that are not yet represented in SI³+ISBA-ES, such as for example the formation of superimposed ice.

Since this study focuses solely on the thermodynamics of snow and sea ice, it serves as a preliminary step towards the full integration of ISBA-ES within SI³ and, subsequently, the CNRM-CM framework. The complete integration of ISBA-ES within SI³ requires the implementation of advection for time-varying snow layers, which is currently in progress. Following this, SI³+ISBA-ES must be coupled with the atmosphere to achieve its full integration within the CNRM-CM framework. This will require additional development to enable the snow model to be driven by atmospheric heat fluxes. In the current code version, these fluxes over snow are calculated within the ISBA-ES model, which is appropriate for a forced mode but not feasible within the existing CNRM-CM coupling approach, where surface heat fluxes are typically calculated in the atmospheric model. To conclude, this paper marks the starting point of developments towards an improved snow over sea ice in the CNRM-CM model.

https://doi.org/10.5194/egusphere-2024-3220
Preprint. Discussion started: 4 February 2025

Aknowledgments

The SHEBA data were provided by NCAR/EOL under the sponsorship of the National Science Foundation. We gratefully acknowledge the SHEBA Atmospheric Surface Flux Group (ASFG), who were responsible for the surface flux measurements during the SHEBA project (E. L. Andreas,C. W. Fairall, P. S. Guest and P. O. G. Persson).

We also gratefully acknowledge Glen Liston and Julienne Stroeve for their providing of the SnowModel-LG data and of the tools to extract the data over the SHEBA area.

This work was supported by a national funding by the Agence Nationale de la Recherche within the framework of the Investissement d'Avenir programme under the ANR-17-MPGA-0003 ASET reference. This article has received funding from the European Union's Horizon 2020 research and innovation programme under grant agreement No 101003826 via project CRiceS (Climate Relevant interactions and feedbacks: the key role of sea ice and Snow in the polar and global climate system).

Code and data availability

For the NEMO model, the version 4.2.0 used in our paper is available on the official NEMO git repository https://forge.nemo-ocean.eu/nemo/nemo/-/tree/4.2.0 and has an associated reference DOI: https://zenodo.org/records/6334656 .

Additional Fortran sources required to compile NEMO/SI3 + ISBAES code over a configuration following the SHEBA trajectory are available at: https://doi.org/10.5281/zenodo.14719233 as well as the namelists used to run the simulations.

The atmospheric and surface forcings used to run the simulations, as well as the scripts used to extract the forcing from ERA5, GLORYS or MERRA2 over the path of the SHEBA experiment can be found at https://doi.org/10.5281/zenodo.14720364 .

The datasets of all simulations used in this paper can be found at: https://doi.org/10.5281/zenodo.14720517 .

The SnowModel-LG datasets are available at http://dx.doi.org/10.5067/27A0P5M6LZBI and the SHEBA snow data are available from the website (http://data.eol.ucar.edu/codiac_data/sheba/data/perovich/ICEWEB/snow.htm).

Competing interests

The contact author has declared that none of the authors has any competing interests.

Author contribution

Théo Brivoal: Writing – review & editing, Writing – original draft, Visualization, Validation, Methodology, Investigation, Formal analysis, Data curation, Conceptualization.

Virginie Guemas: Writing – review & editing, Supervision, Methodology, Funding acquisition, technical and scientific support.

Martin Vancoppenole: Writing – review & editing, technical and scientific support.

https://doi.org/10.5194/egusphere-2024-3220
Preprint. Discussion started: 4 February 2025

Clément Rousset: Writing – review & editing, technical and scientific support.

Bertrand Decharme: Writing – review & editing, technical and scientific support.

References

Anderson, E. A.: A Point Energy and Mass Balance Model of a Snow Cover, U.S. Department of Commerce, National Oceanic and Atmospheric Administration, National Weather Service, Office of Hydrology, 172 pp., 1976.

Bitz, C. M. and Lipscomb, W. H.: An energy-conserving thermodynamic model of sea ice, J. Geophys. Res. Oceans, 104, 15669–15677, https://doi.org/10.1029/1999JC900100, 1999.

Bitz, C. M., Holland, M. M., Weaver, A. J., and Eby, M.: Simulating the ice-thickness distribution in a coupled climate model, J. Geophys. Res. Oceans, 106, 2441–2463, https://doi.org/10.1029/1999JC000113, 2001.

Bohren, C. F. and Beschta, R. L.: Snowpack albedo and snow density, Cold Reg. Sci. Technol., 1, 47–50, https://doi.org/10.1016/0165-232X(79)90018-1, 1979.

Boone, A.: Description du Schema de Neige ISBA-ES (Explicit Snow), 2002.

Boone, A. and Etchevers, P.: An Intercomparison of Three Snow Schemes of Varying Complexity Coupled to the Same Land Surface Model: Local-Scale Evaluation at an Alpine Site, 2001.

Brun, E., Martin, E., Simon, V., Gendre, C., and Coleou, C.: An Energy and Mass Model of Snow Cover Suitable for Operational Avalanche Forecasting, J. Glaciol., 35, 333–342, https://doi.org/10.3189/S0022143000009254, 1989.

Brun, E., Martin, E., and Spiridonov, V.: Coupling a multi-layered snow model with a GCM, Ann. Glaciol., 25, 66–72, https://doi.org/10.3189/S0260305500013811, 1997.

Decharme, B., Brun, E., Boone, A., Delire, C., Le Moigne, P., and Morin, S.: Impacts of snow and organic soils parameterization on northern Eurasian soil temperature profiles simulated by the ISBA land surface model, The Cryosphere, 10, 853–877, https://doi.org/10.5194/tc-10-853-2016, 2016.

Domine, F., Barrere, M., and Sarrazin, D.: Seasonal evolution of the effective thermal conductivity of the snow and the soil in high Arctic herb tundra at Bylot Island, Canada, The Cryosphere, 10, 2573–2588, https://doi.org/10.5194/tc-10-2573-2016, 2016.

Domine, F., Gauthier, G., Vionnet, V., Fauteux, D., Dumont, M., and Barrere, M.: Snow physical properties may be a significant determinant of lemming population dynamics in the high Arctic, Arct. Sci., 4, 813–826, https://doi.org/10.1139/as-2018-0008, 2018.

Fichefet, T. and Maqueda, M. A. M.: Sensitivity of a global sea ice model to the treatment of ice thermodynamics and dynamics, J. Geophys. Res. Oceans, 102, 12609–12646, https://doi.org/10.1029/97JC00480, 1997.

https://doi.org/10.5194/egusphere-2024-3220
Preprint. Discussion started: 4 February 2025

Fichefet, T., Tartinville, B., and Goosse, H.: Sensitivity of the Antarctic sea ice to the thermal conductivity of snow, Geophys. Res. Lett., 27, 401–404, https://doi.org/10.1029/1999GL002397, 2000.

Gelaro, R., McCarty, W., Suárez, M. J., Todling, R., Molod, A., Takacs, L., Randles, C., Darmenov, A., Bosilovich, M. G., Reichle, R., Wargan, K., Coy, L., Cullather, R., Draper, C., Akella, S., Buchard, V., Conaty, A., da Silva, A., Gu, W., Kim, G.-K., Koster, R., Lucchesi, R., Merkova, D., Nielsen, J. E., Partyka, G., Pawson, S., Putman, W., Rienecker, M., Schubert, S. D., Sienkiewicz, M., and Zhao, B.: The Modern-Era Retrospective Analysis for Research and Applications, Version 2 (MERRA-2), J. Clim., Volume 30, 5419–5454, https://doi.org/10.1175/JCLI-D-16-0758.1, 2017.

Gurvan, M., Bourdallé-Badie, R., Chanut, J., Clementi, E., Coward, A., Ethé, C., Iovino, D., Lea, D., Lévy, C., Lovato, T., Martin, N., Masson, S., Mocavero, S., Rousset, C., Storkey, D., Müeller, S., Nurser, G., Bell, M., Samson, G., Mathiot, P., Mele, F., and Moulin, A.: NEMO ocean engine, https://doi.org/10.5281/zenodo.6334656, 2022.

Hersbach, H., Bell, B., Berrisford, P., Hirahara, S., Horányi, A., Muñoz-Sabater, J., Nicolas, J., Peubey, C., Radu, R., Schepers, D., Simmons, A., Soci, C., Abdalla, S., Abellan, X., Balsamo, G., Bechtold, P., Biavati, G., Bidlot, J., Bonavita, M., De Chiara, G., Dahlgren, P., Dee, D., Diamantakis, M., Dragani, R., Flemming, J., Forbes, R., Fuentes, M., Geer, A., Haimberger, L., Healy, S., Hogan, R. J., Hólm, E., Janisková, M., Keeley, S., Laloyaux, P., Lopez, P., Lupu, C., Radnoti, G., de Rosnay, P., Rozum, I., Vamborg, F., Villaume, S., and Thépaut, J.-N.: The ERA5 global reanalysis, Q. J. R. Meteorol. Soc., 146, 1999–2049, https://doi.org/10.1002/qj.3803, 2020.

Holland, M. M., Clemens-Sewall, D., Landrum, L., Light, B., Perovich, D., Polashenski, C., Smith, M., and Webster, M.: The influence of snow on sea ice as assessed from simulations of CESM2, The Cryosphere, 15, 4981–4998, https://doi.org/10.5194/tc-15-4981-2021, 2021.

Jafari, M. and Lehning, M.: Convection of snow: when and why does it happen?, Front. Earth Sci., 11, https://doi.org/10.3389/feart.2023.1167760, 2023.

Jutras, M., Vancoppenolle, M., Lourenço, A., Vivier, F., Carnat, G., Madec, G., Rousset, C., and Tison, J.-L.: Thermodynamics of slush and snow–ice formation in the Antarctic sea-ice zone, Deep Sea Res. Part II Top. Stud. Oceanogr., 131, 75–83, https://doi.org/10.1016/j.dsr2.2016.03.008, 2016.

Kojima, K.: Densification of Seasonal Snow Cover, Phys. Snow Ice Proc., 1, 929–952, 1967.

Kondo, J. and Yamazaki, T.: A Prediction Model for Snowmelt, Snow Surface Temperature and Freezing Depth Using a Heat Balance Method, 1990.

Large, W. and Yeager, S.: Diurnal to decadal global forcing for ocean and sea-ice models: The data sets and flux climatologies, UCAR/NCAR, https://doi.org/10.5065/D6KK98Q6, 2004.

Le Moigne, P., Besson, F., Martin, E., Boé, J., Boone, A., Decharme, B., Etchevers, P., Faroux, S., Habets, F., Lafaysse, M., Leroux, D., and Rousset-Regimbeau, F.: The latest improvements with SURFEX v8.0 of the Safran–Isba–Modcou hydrometeorological model for France, Geosci. Model Dev., 13, 3925–3946, https://doi.org/10.5194/gmd-13-3925-2020, 2020.

Lecomte, O., Fichefet, T., Vancoppenolle, M., Domine, F., Massonnet, F., Mathiot, P., Morin, S., and Barriat, P. y.: On the formulation of snow thermal conductivity in large-scale sea ice models, J. Adv. Model. Earth Syst., 5, 542–557, https://doi.org/10.1002/jame.20039, 2013.

Lellouche, J.-M., Greiner, E., Le Galloudec, O., Garric, G., Regnier, C., Drevillon, M., Benkiran, M., Testut, C.-E., Bourdalle-Badie, R., Gasparin, F., Hernandez, O., Levier, B., Drillet, Y., Remy, E., and Le Traon, P.-Y.: Recent updates to the Copernicus

https://doi.org/10.5194/egusphere-2024-3220
Preprint. Discussion started: 4 February 2025

Marine Service global ocean monitoring and forecasting real-time 1⁄12° high-resolution system, Ocean Sci., 14, 1093–1126, https://doi.org/10.5194/os-14-1093-2018, 2018.

Leonard, K. C. and Maksym, T.: The importance of wind-blown snow redistribution to snow accumulation on Bellingshausen Sea ice, Ann. Glaciol., 52, 271–278, https://doi.org/10.3189/172756411795931651, 2011.

Liston, G. E., Itkin, P., Stroeve, J., Tschudi, M., Stewart, J. S., Pedersen, S. H., Reinking, A. K., and Elder, K.: A Lagrangian Snow-Evolution System for Sea-Ice Applications (SnowModel-LG): Part I—Model Description, J. Geophys. Res. Oceans, 125, e2019JC015913, https://doi.org/10.1029/2019JC015913, 2020.

Loth, B., Graf, H.-F., and Oberhuber, J. M.: Snow cover model for global climate simulations, J. Geophys. Res. Atmospheres, 98, 10451–10464, https://doi.org/10.1029/93JD00324, 1993.

Lynch-Stieglitz, M.: The Development and Validation of a Simple Snow Model for the GISS GCM, 1994.

Mellor, M.: Properties of snow, 1964.

Nicolaus, M., Haas, C., and Bareiss, J.: Observations of superimposed ice formation at melt-onset on fast ice on Kongsfjorden, Svalbard, Phys. Chem. Earth Parts ABC, 28, 1241–1248, https://doi.org/10.1016/j.pce.2003.08.048, 2003.

Pahaut, E.: Les cristaux de neige et leurs métamorphoses (), Centre d'étude de la neige, 58 pp., 1975.

Perovich, D. K. and Polashenski, C.: Albedo evolution of seasonal Arctic sea ice, Geophys. Res. Lett., 39, https://doi.org/10.1029/2012GL051432, 2012.

Perovich, D. K., Grenfell, T. C., Light, B., Richter-Menge, J. A., Sturm, M., Tucker III, W. B., Eicken, H., Maykut, G. A., and Elder, B.: SHEBA: Snow and Ice Studies CD-ROM, 1999.

Persson, P. O. G., Fairall, C. W., Andreas, E. L., Guest, P. S., and Perovich, D. K.: Measurements near the Atmospheric Surface Flux Group tower at SHEBA: Near-surface conditions and surface energy budget, J. Geophys. Res. Oceans, 107, SHE 21-1-SHE 21-35, https://doi.org/10.1029/2000JC000705, 2002.

Petty, A. A., Webster, M., Boisvert, L., and Markus, T.: The NASA Eulerian Snow on Sea Ice Model (NESOSIM) v1.0: initial model development and analysis, Geosci. Model Dev., 11, 4577–4602, https://doi.org/10.5194/gmd-11-4577-2018, 2018.

Royer, A., Picard, G., Vargel, C., Langlois, A., Gouttevin, I., and Dumont, M.: Improved Simulation of Arctic Circumpolar Land Area Snow Properties and Soil Temperatures, Front. Earth Sci., 9, https://doi.org/10.3389/feart.2021.685140, 2021.

Sommer, C. G., Lehning, M., and Fierz, C.: Wind Tunnel Experiments: Influence of Erosion and Deposition on Wind-Packing of New Snow, Front. Earth Sci., 6, https://doi.org/10.3389/feart.2018.00004, 2018.

Stroeve, J., Liston, G. E., Buzzard, S., Zhou, L., Mallett, R., Barrett, A., Tschudi, M., Tsamados, M., Itkin, P., and Stewart, J. S.: A Lagrangian Snow Evolution System for Sea Ice Applications (SnowModel-LG): Part II—Analyses, J. Geophys. Res. Oceans, 125, e2019JC015900, https://doi.org/10.1029/2019JC015900, 2020.

Sturm, M. and Benson, C. S.: Vapor transport, grain growth and depth-hoar development in the subarctic snow, J. Glaciol., 43, 42–59, https://doi.org/10.3189/S0022143000002793, 1997.

Sturm, M. and Massom, R. A.: Snow in the sea ice system: friend or foe?, in: Sea Ice, John Wiley & Sons, Ltd, 65–109, https://doi.org/10.1002/9781118778371.ch3, 2017.

https://doi.org/10.5194/egusphere-2024-3220
Preprint. Discussion started: 4 February 2025

Sturm, M., Holmgren, J., König, M., and Morris, K.: The thermal conductivity of seasonal snow, J. Glaciol., 43, 26–41, https://doi.org/10.3189/S0022143000002781, 1997.

Sturm, M., Holmgren, J., and Perovich, D. K.: Winter snow cover on the sea ice of the Arctic Ocean at the Surface Heat Budget of the Arctic Ocean (SHEBA): Temporal evolution and spatial variability, J. Geophys. Res. Oceans, 107, SHE 23-1-SHE 23-17, https://doi.org/10.1029/2000JC000400, 2002.

Sun, S., Jin, J., and Xue, Y.: A simple snow-atmosphere-soil transfer model, J. Geophys. Res. Atmospheres, 104, 19587–19597, https://doi.org/10.1029/1999JD900305, 1999.

Thorndike, A. S., Rothrock, D. A., Maykut, G. A., and Colony, R.: The thickness distribution of sea ice, J. Geophys. Res. 1896-1977, 80, 4501–4513, https://doi.org/10.1029/JC080i033p04501, 1975.

Vancoppenolle, M., Fichefet, T., Goosse, H., Bouillon, S., Madec, G., and Maqueda, M. A. M.: Simulating the mass balance and salinity of Arctic and Antarctic sea ice. 1. Model description and validation, Ocean Model., 27, 33–53, https://doi.org/10.1016/j.ocemod.2008.10.005, 2009.

Vancoppenolle, M., Rousset, C., Blockley, E., Aksenov, Y., Feltham, D., Fichefet, T., Garric, G., Guémas, V., Iovino, D., Keeley, S., Madec, G., Massonnet, F., Ridley, J., Schroeder, D., and Tietsche, S.: SI3, the NEMO Sea Ice Engine, https://doi.org/10.5281/zenodo.7534900, 2023.

Voldoire, A., Sanchez-Gomez, E., Salas y Mélia, D., Decharme, B., Cassou, C., Sénési, S., Valcke, S., Beau, I., Alias, A., Chevallier, M., Déqué, M., Deshayes, J., Douville, H., Fernandez, E., Madec, G., Maisonnave, E., Moine, M.-P., Planton, S., Saint-Martin, D., Szopa, S., Tyteca, S., Alkama, R., Belamari, S., Braun, A., Coquart, L., and Chauvin, F.: The CNRM-CM5.1 global climate model: description and basic evaluation, Clim. Dyn., 40, 2091–2121, https://doi.org/10.1007/s00382-011-1259-y, 2013.

Webster, M., Gerland, S., Holland, M., Hunke, E., Kwok, R., Lecomte, O., Massom, R., Perovich, D., and Sturm, M.: Snow in the changing sea-ice systems, Nat. Clim. Change, 8, 946–953, https://doi.org/10.1038/s41558-018-0286-7, 2018.

Wever, N., Rossmann, L., Maaß, N., Leonard, K. C., Kaleschke, L., Nicolaus, M., and Lehning, M.: Version 1 of a sea ice module for the physics-based, detailed, multi-layer SNOWPACK model, Geosci. Model Dev., 13, 99–119, https://doi.org/10.5194/gmd-13-99-2020, 2020.